Simplifying Prostate Elastography Using Micro-ultrasound and Transfer Function Imaging

Reid Vassallo[1(✉)], Tajwar Abrar Aleef[1,2], Vedanth Desaigoudar[1], Qi Zeng[3,4], David Black[3], Brian Wodlinger[5], Miles Mannas[6], Peter C. Black[6], and Septimiu E. Salcudean[1,3,6]

[1] School of Biomedical Engineering, University of British Columbia, Vancouver, BC, Canada
rvassallo@prostatecentre.com
[2] Synthesis Health, Maple Ridge, BC, Canada
[3] Department of Electrical and Computer Engineering, University of British Columbia, Vancouver, BC, Canada
[4] Boston Children's Hospital, Harvard Medical School, Cambridge, MA, USA
[5] Exact Imaging, Markham, ON, Canada
[6] Department of Urologic Sciences, University of British Columbia, Vancouver, BC, Canada

Abstract. Prostate cancer is one of the most commonly diagnosed cancers worldwide, yet working towards more accurate and cost-effective detection strategies for this disease remains an active area of research. This includes introducing a new method called micro-ultrasound (microUS), which has equal performance to the gold standard multiparametric magnetic resonance imaging for prostate biopsy guidance. Cancerous lesions are often stiffer than their healthy surroundings, and this tissue stiffness can be imaged using elastography. Clinical strain elastography generally uses manual compression of the tissue via the probe face; however, this method is highly user-dependent and can result in unreliable images due to the complexity and steep learning curve to apply ideal compression. Here, we implement and validate a relative elastography method called transfer function (TF) imaging, which uses automatic tissue compression from a voice coil motor attached to the microUS probe for excitation, and calculates the tissue's relative stiffness from its frequency response to this excitation. We demonstrate our method's improved repeatability compared to manual strain elastography using quantitative and qualitative evaluations performed using a commercial quality assurance elasticity phantom. Overall, this method makes elastography much simpler for clinicians, further enabling its use in guiding prostate biopsy procedures.

Keywords: Micro-ultrasound · Elastography · Prostate cancer

A. Gomez et al. (Eds.): ASMUS 2024, LNCS 15186, pp. 14–23, 2025.
https://doi.org/10.1007/978-3-031-73647-6_2

1 Introduction

Prostate cancer (PCa) is the fourth most commonly diagnosed cancer worldwide [5], with rates expected to rise until 2040 due in part to an aging population and rising life expectancy worldwide [10]. However, despite its relatively high prevalence, limitations persist in the detection and diagnosis of this disease. Many of these limitations can be traced back to the inability of conventional ultrasound (US) to accurately and reliably identify PCa tumours, as only approximately 50% of PCa lesions are detectable by US [17]. This results in a series of biopsy samples being taken from predefined locations in the prostate to search for the disease, rather than targeting specific suspicious areas [15]. In turn, this systematic sampling technique leads to some cases of clinically significant PCa going undetected, as well as clinically insignificant PCa being overdiagnosed [9]. Together, this results in a relatively poor sensitivity of 48% [1]. Addressing this shortcoming has been an active area of research, and has led to multiparametric magnetic resonance imaging (mpMRI) becoming the gold standard for PCa imaging. However, mpMRI remains an expensive and relatively inaccessible method for disease detection. Another effort to improve this has been the development of the ExactVu™ micro-ultrasound (microUS) system (Exact Imaging, Markham, ON, Canada), which uses a higher transmit frequency of up to 29 MHz (compared to typical 9–12 MHz [11]), allowing it to have an improved spatial resolution of up to 70 μm [6]. Meta-analyses have shown that B-mode microUS alone can guide targeted prostate biopsies as well as mpMRI [24], although a randomized controlled trial is underway to confirm these findings (NCT05220501) [12]. There has recently been additional work to further improve the utility of microUS, including deep learning-based image analysis [20], quantitative US [18], volumetric imaging [23], and elastography [3].

Since tumours are often stiffer than their surrounding healthy tissue [22], elastography using conventional US has been an active area of development for PCa imaging [2,4]. US-based elastography has been a component of previous multiparametric US systems, and contributed to these systems being able to detect PCa better than B-mode alone [13].

A popular method of US-based elastography is shear wave elastography, which provides quantitative estimates of tissue stiffness [2,4]. However, these estimates are only valid if a volumetric image is obtained due to the unknown shear wave direction in the tissue [26]. This makes it difficult to obtain these images in real-time to guide prostate biopsy procedures, as the geometric constraints of a transrectal US (TRUS) probe mean that a matrix array to obtain real-time three dimensional (3D) images are not yet available, and working around this requires additional complexity. However, when trying to pinpoint suspicious areas for PCa in a patient, it is sufficient to be able to identify areas which are relatively stiffer than their surrounding tissue rather than requiring specific quantitative values of absolute stiffness. This relative stiffness information can be provided by strain elastography, which is a technically simpler method.

Current implementations of strain elastography using microUS have relied on manual tissue compression using the probe face, but this is known to have higher

inter-observer variability than automated methods [16] due to its complexity and steep learning curve. In an effort to overcome this known limitation of strain elastography, it has previously been demonstrated that relative tissue stiffness can be elucidated from the transfer function (TF) of the tissue's response to an automatically generated vibration [8], even being implemented in real-time [19]. This simplification of the method can allow for much less user-dependent stiffness imaging, which could make it much easier to be clinically adopted.

In this work, the TF elastography method is implemented for the first time using the ExactVu™ microUS system, using a probe-mounted voice coil motor for tissue excitation. The repeatability of this method (as a measure of simplicity for the user) is compared against manual strain elastography using the ExactVu™ using a commercial quality assurance phantom. In summary, the main contributions of this work are: the first implementation of TF-based elastography using microUS and the first integration of probe-mounted voice coil-drive multi-frequency excitation for strain imaging using microUS.

2 Methods

2.1 System Overview

Hardware Setup. To acquire freehand elastography images, some additional hardware is required with the ExactVu™ microUS system. The tissue is excited with a linear voice coil motor which is rigidly affixed to the TRUS probe such that the direction of motion is approximately perpendicular to the imaging array. The excitation frequencies and their relative phases are controlled by a function generator (33220A, Agilent Technologies, USA), and amplified by a previously described custom control box, [4], which uses a Lepy LP-2020A signal amplifier (Lepai, Shenzhen, China). The overall intensity of the signal, and thus the tissue excitation, can be changed by using either a physical knob on the control box or within the custom software controlling the function generator. This setup can be seen in Fig. 1.

Imaging and Excitation Parameters. The voice coil is driven using a sum of sinusoids from 1–10 Hz, with phase offsets chosen to produce a waveform without major constructive interference between the frequencies such that the local maxima are relatively uniform in amplitude. To do so, the phase offsets were sampled randomly from a uniform distribution between 0 and 2π until the above condition was met. These same phase offsets were then used for every imaging session. This excitation can be described as:

$$\sum_{n=1}^{10} sin(2\pi nt + \theta_n) \tag{1}$$

where t represents time (in seconds) and θ_n represents the phase offset for each frequency.

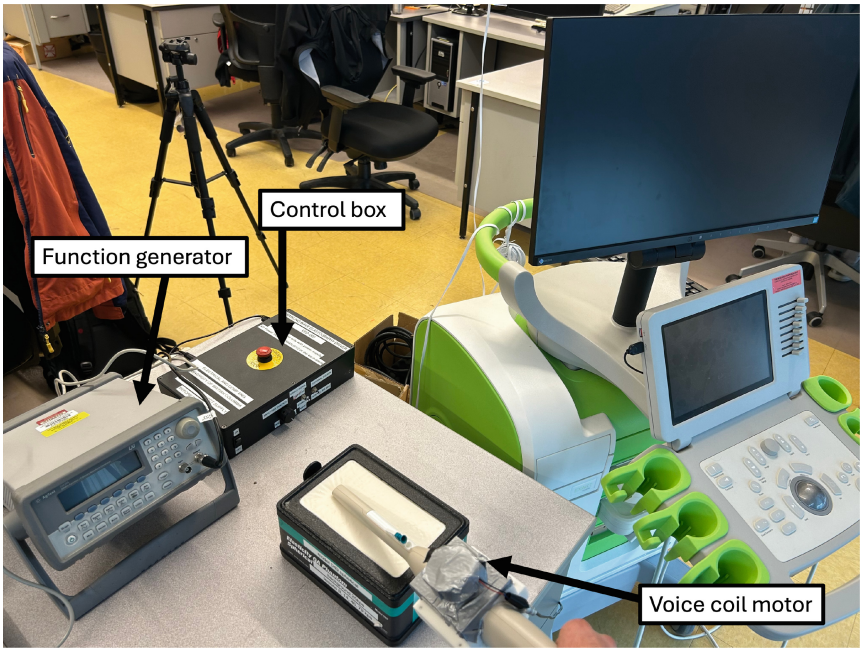

Fig. 1. Our imaging setup including the ExactVu™ microUS device, imaging phantom, and mechanical excitation hardware.

The majority of PCa tumours occur in the peripheral zone [14], which should be sufficiently covered by the imaging depth of 30 mm chosen for this work. A single focal zone was used, set at approximately 25 mm. Our choice of settings resulted in a frame rate of 25 Hz, ensuring that even our maximum excitation frequency (10 Hz) fell below the Nyquist frequency for this frame rate (12.5 Hz). The cine capture feature of the ExactVu™ system was used, and the radiofrequency (RF) data was saved and transmitted automatically over the network to another computer for immediate processing and display.

Image Processing. Tissue displacement is tracked in the RF images using a speckle tracking algorithm [25], and this was then used to calculate the frequency response of the tissue to estimate relative elasticity values, as described below.

The mechanical properties of tissue can be modelled by a one-dimensional model of springs, dampers, and masses which are assembled as Voigt elements, as previously explored in [7]. If this linear network is excited by a waveform consisting of a single frequency, we expect the displacements and local strains will maintain the same frequency, but have different amplitudes and phase lags. This will hold true if the excitation consists of multiple frequencies, as in our case, and the spectra of displacements and strains will cover the same range of frequencies as the input.

The TF between the applied force and displacements has been previously studied [21], including the case where the applied force cannot be accurately measured. In this case, the displacements are taken relative to a common reference location in the image. When this common reference location, arbitrarily chosen as the center of the image in our case, is defined as element j, and the ith element is the block of pixels currently under investigation, the TF of this system is defined as:

$$H_i^j(\omega) = \frac{P_{x_i x_j}(\omega)}{P_{x_i x_i}(\omega)} \tag{2}$$

where $P_{x_i x_i}(\omega)$ is the power spectral density of element $x_i(t)$, and $P_{x_i x_j}(\omega)$ is the cross-spectral density between elements i and j.

Tissue stiffness can be estimated by averaging the magnitude of this TF over a range of low frequencies where it is approximately constant. Here, we calculated the TF, $H_i^j(\omega)$, using 20 image frames. Each patch used for analysis was 28 RF samples in the axial direction, with 50% overlap.

Manual Strain Imaging. To validate TF imaging using microUS, we compared it to manual strain imaging, which has been previously implemented on the ExactVu™ system [3]. To briefly recap this previous implementation, compression was manually applied using the probe face at a frequency of approximately 1 Hz, and tissue displacement (δ) was tracked using the same speckle tracking algorithm as our TF method [25]. The strain (ϵ) was then calculated by finding the spatial derivative of $|\delta|$ along the axial direction of each RF line, described by

$$\epsilon = \frac{d|\delta|}{dx} \tag{3}$$

A Gaussian smoothing filter with an anisotropic kernel (with sigma values of 5 along the x axis and 3 along the y axis) was applied to ϵ in an effort to reduce noise in the resulting image.

2.2 Phantom Validation

Validation of this method was performed using a commercial quality assurance elasticity phantom, namely the CIRS 049 (Computerized Imaging Reference Systems, Norfolk, VA, USA). Imaging was performed on its four small (10 mm diameter) spherical inclusions. The stiffness of each inclusion increases from Type 1 to Type 4, with Type 4 being the stiffest. Imaging was performed freehand in order to best mimic the expected future clinical environment.

Results are based on 10 acquisitions using the TF method and 3 acquisitions (each consisting of 59 frames) using manual compression for each inclusion.

Quantitative Evaluation. We compared our TF method to manual strain imaging using strain ratio (SR) and contrast to noise ratio (CNR), as defined in [3], in order to obtain a pseudo-quantitative assessment of the resulting images.

The interquartile range (IQR), which is the difference between the 75th and 25th percentile values, of these two metrics (SR and CNR) were calculated and are presented in Table 1.

The inclusion and background were manually segmented in MATLAB (The Mathworks, Natick, MA, USA), where the inclusion was a circular region of interest (ROI) drawn to include the spherical inclusion's imaged cross section, and the background ROI was a rectangle in a representative section of the image to one side of the inclusion. These were drawn for each TF image output, but because of the high variability in manual strain images, as seen in Fig. 3, the segmentation was done on the best frame of the series and then mapped to the remaining 58 strain elastography frames.

Qualitative Evaluation. Qualitative evaluation between manual strain and TF imaging was performed by comparing the best and worst images from each method, to get a sense of the variability in the images. The determination of the best and worst frames was done subjectively by considering how visible the inclusions were in each frame.

3 Results

3.1 Quantitative Evaluation

The results of our quantitative evaluation are shown graphically in Fig. 2, and IQR values are shown in Table 1. In almost all cases the inter-image variability, as determined by the IQR for SR and CNR measurements, is demonstrably better for our TF method.

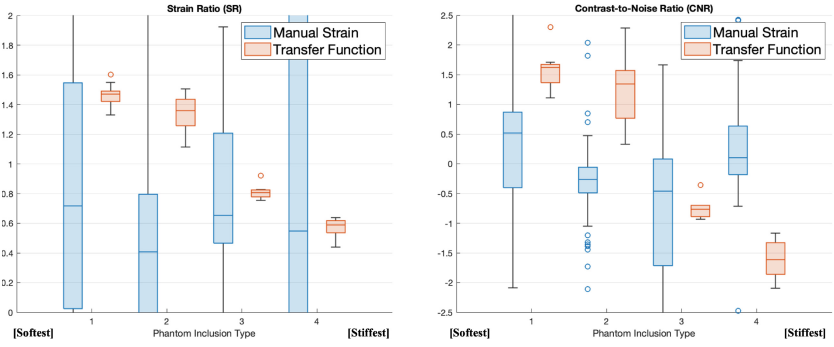

Fig. 2. Boxplots comparing the SR and CNR values of the same phantom inclusions imaged using our proposed TF based method and previously published manual strain elastography using ExactVu™ microUS. IQR values of these boxplots are shown in Table 1

Table 1. Interquartile range (IQR) values for four inclusions, imaged with both elastography methods. The lower IQR for each inclusion is bolded.

	Strain Ratio IQR		Contrast to Noise Ratio IQR	
	Transfer Function	Manual	Transfer Function	Manual
Inclusion 1	**0.07**	1.52	**0.30**	1.27
Inclusion 2	**0.18**	1.69	0.80	**0.43**
Inclusion 3	**0.05**	0.74	**0.19**	1.79
Inclusion 4	**0.08**	2.87	**0.54**	0.82

3.2 Qualitative Evaluation

A qualitative comparison of the best and worst frames for TF and manual strain imaging can be seen in Fig. 3. To further highlight the improved repeatability of our TF method, the display parameters were kept constant between all four displayed TF images, but were adjusted for the manual strain images individually to match the contrast of the TF images for display purposes.

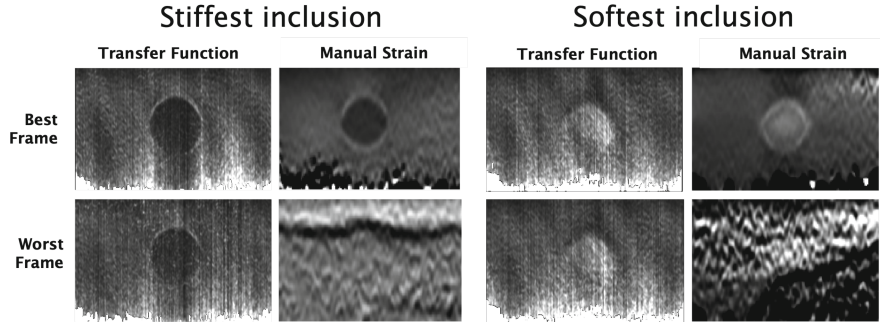

Fig. 3. A qualitative comparison of the best and worst frames acquired using the TF and manual strain methods for the softest and stiffest inclusions. This demonstrates the improved repeatability of the TF method, as compared to manual strain elastography.

4 Discussion

In this work we describe and validate the first known implementation of TF-based elastography using the ExactVu™ microUS system in order to simplify the acquisition of elastography images for PCa detection. We demonstrate its ability to accurately identify inclusions which have different mechanical properties than their surroundings, and particularly that it can do this with less variability between images than manual strain elastography, and should require less user

training. As can be seen in Fig. 3, this system is more effective at identifying inclusions which are stiffer than their surroundings, rather than lesions which are softer. This has relevance to our proposed clinical application of PCa detection, as cancers tend to be stiffer than their surroundings, rather than softer [22]. Although a major component of the novelty of this work is the implementation of TF imaging using state-of-the-art microUS, this method can be implemented on any system which can provide access to RF image data.

4.1 Limitations

There are some limitations to this study, which are necessitated by the differences between TF-based and manual strain elastography. The TF method uses a series of 20 frames to calculate the frequency response of the tissue. However, manual strain just uses the displacement measured between two adjacent frames in the time series. Having more frames included in each TF image may inherently improve its reliability as a form of averaging, but we were unable to control for this effectively since it is part of the proposed benefit of this method.

4.2 Future Work

Future work will include optimization of this method to allow for real-time implementation, such that it can be used to guide prostate biopsy procedures. We also plan to integrate the voice coil motor into a system similar to the one proposed in [4] for clinical imaging. It has also been shown that the phase of the TF can be used to determine the viscosity of the tissue under investigation [7], which can provide an additional parameter to identify areas suspicious for harbouring PCa.

5 Conclusion

We demonstrate the first implementation of TF-based strain imaging using microUS. We compared this to previously-published manual strain elastography using the same microUS system using both quantitative and qualitative methods, demonstrating our method's improved repeatability, which we expect will allow for better eventual clinical adoption.

Acknowledgments. This work was funded by the Canadian Institutes of Health Research (CIHR) and the Natural Sciences and Engineering Research Council (NSERC) through a CHRP grant. We also acknowledge the support from the Charles A. Lazlo Chair in Biomedical Engineering held by Professor Salcudean.

Disclosure of Interests. Brian Wodlinger is employed by Exact Imaging, creators of the ExactVu™ system. All other authors have no competing interests to declare.

References

1. Ahmed, H.U., Bosaily, A.E.S., Brown, L.C., Gabe, R., Kaplan, R., Parmar, M.K., Collaco-Moraes, Y., Ward, K., Hindley, R.G., Freeman, A., et al.: Diagnostic accuracy of multi-parametric mri and trus biopsy in prostate cancer (promis): a paired validating confirmatory study. The Lancet **389**(10071), 815–822 (2017)
2. Aleef, T.A., Lobo, J., Baghani, A., Mohammed, S., Eskandari, H., Moradi, H., Rohling, R., Goldenberg, S.L., Morris, W.J., Mahdavi, S.S., et al.: Multi-frequency 3d shear wave absolute vibro-elastography (s-wave) system for the prostate. IEEE Transactions on Medical Imaging (2023)
3. Aleef, T.A., Vassallo, R., Zeng, Q., Mahdavi, S.S., Wodlinger, B., Mannas, M., Black, P.C., Salcudean, S.E.: Implementation of shear wave and strain elastography with micro-ultrasound. In: 2023 IEEE International Ultrasonics Symposium (IUS). pp. 1–6. IEEE (2023)
4. Aleef, T.A., Zeng, Q., Moradi, H., Mohammed, S., Curran, T., Honarvar, M., Rohling, R., Mahdavi, S.S., Salcudean, S.E.: 3d transducer mounted shear wave absolute vibro-elastography: Proof of concept. IEEE Transactions on Ultrasonics, Ferroelectrics, and Frequency Control (2023)
5. Bray, F., Laversanne, M., Sung, H., Ferlay, J., Siegel, R.L., Soerjomataram, I., Jemal, A.: Global cancer statistics 2022: Globocan estimates of incidence and mortality worldwide for 36 cancers in 185 countries. CA: a cancer journal for clinicians **74**(3), 229–263 (2024)
6. Dias, A.B., O'Brien, C., Correas, J.M., Ghai, S.: Multiparametric ultrasound and micro-ultrasound in prostate cancer: a comprehensive review. The British Journal of Radiology **95**(1131), 20210633 (2022)
7. Eskandari, H., Salcudean, S.E., Rohling, R.: Viscoelastic parameter estimation based on spectral analysis. IEEE transactions on ultrasonics, ferroelectrics, and frequency control **55**(7), 1611–1625 (2008)
8. Eskandari, H., Salcudean, S.E., Rohling, R., Baghani, A., Frew, S., Gordon, P.B., Warren, L.: Identifying malignant and benign breast lesions using vibroelastography. In: 2013 IEEE International Ultrasonics Symposium (IUS). pp. 25–28. IEEE (2013)
9. Grossman, D.C., Curry, S.J., Owens, D.K., Bibbins-Domingo, K., Caughey, A.B., Davidson, K.W., Doubeni, C.A., Ebell, M., Epling, J.W., Kemper, A.R., et al.: Screening for prostate cancer: Us preventive services task force recommendation statement. Jama **319**(18), 1901–1913 (2018)
10. James, N.D., Tannock, I., N'Dow, J., Feng, F., Gillessen, S., Ali, S.A., Trujillo, B., Al-Lazikani, B., Attard, G., Bray, F., et al.: The lancet commission on prostate cancer: planning for the surge in cases. The Lancet **403**(10437), 1683–1722 (2024)
11. Klotz, C.L.: Can high resolution micro-ultrasound replace mri in the diagnosis of prostate cancer? European urology focus **6**(2), 419–423 (2020)
12. Klotz, L., Andriole, G., Cash, H., Cooperberg, M., Crawford, E.D., Emberton, M., Gomez-Sancha, F., Klein, E., Lughezzani, G., Marks, L., et al.: Optimization of prostate biopsy-micro-ultrasound versus mri (optimum): A 3-arm randomized controlled trial evaluating the role of 29 mhz micro-ultrasound in guiding prostate biopsy in men with clinical suspicion of prostate cancer. Contemporary Clinical Trials **112**, 106618 (2022)
13. Mannaerts, C.K., Wildeboer, R.R., Remmers, S., van Kollenburg, R.A., Kajtazovic, A., Hagemann, J., Postema, A.W., van Sloun, R.J., J. Roobol, M., Tilki, D., et al.: Multiparametric ultrasound for prostate cancer detection and localization:

correlation of b-mode, shear wave elastography and contrast enhanced ultrasound with radical prostatectomy specimens. The Journal of urology **202**(6), 1166–1173 (2019)
14. McNeal, J.E., Redwine, E.A., Freiha, F.S., Stamey, T.A.: Zonal distribution of prostatic adenocarcinoma: correlation with histologic pattern and direction of spread. The American journal of surgical pathology **12**(12), 897–906 (1988)
15. Mottet, N., Bellmunt, J., Bolla, M., Briers, E., Cumberbatch, M.G., De Santis, M., Fossati, N., Gross, T., Henry, A.M., Joniau, S., et al.: Eau-estro-siog guidelines on prostate cancer. part 1: screening, diagnosis, and local treatment with curative intent. European urology **71**(4), 618–629 (2017)
16. Mulabecirovic, A., Vesterhus, M., Gilja, O.H., Havre, R.F.: In vitro comparison of five different elastography systems for clinical applications, using strain and shear wave technology. Ultrasound in medicine & biology **42**(11), 2572–2588 (2016)
17. Ohori, M., Kattan, M.W., Utsunomiya, T., Suyama, K., Scardino, P.T., Wheeler, T.M.: Do impalpable stage t1c prostate cancers visible on ultrasound differ from those not visible? The Journal of urology **169**(3), 964–968 (2003)
18. Rohrbach, D., Wodlinger, B., Wen, J., Mamou, J., Feleppa, E.: High-frequency quantitative ultrasound for imaging prostate cancer using a novel micro-ultrasound scanner. Ultrasound in medicine & biology **44**(7), 1341–1354 (2018)
19. Salcudean, S.E., French, D., Bachmann, S., Zahiri-Azar, R., Wen, X., Morris, W.J.: Viscoelasticity modeling of the prostate region using vibro-elastography. In: Medical Image Computing and Computer-Assisted Intervention–MICCAI 2006: 9th International Conference, Copenhagen, Denmark, October 1-6, 2006. Proceedings, Part I 9. pp. 389–396. Springer (2006)
20. Shao, Y., Wang, J., Wodlinger, B., Salcudean, S.E.: Improving prostate cancer (pca) classification performance by using three-player minimax game to reduce data source heterogeneity. IEEE Transactions on Medical Imaging **39**(10), 3148–3158 (2020)
21. Turgay, E., Salcudean, S., Rohling, R.: Identifying the mechanical properties of tissue by ultrasound strain imaging. Ultrasound in medicine & biology **32**(2), 221–235 (2006)
22. Tuxhorn, J.A., Ayala, G.E., Smith, M.J., Smith, V.C., Dang, T.D., Rowley, D.R.: Reactive stroma in human prostate cancer: induction of myofibroblast phenotype and extracellular matrix remodeling. Clinical Cancer Research **8**(9), 2912–2923 (2002)
23. Vassallo, R., Aleef, T.A., Zeng, Q., Wodlinger, B., Black, P.C., Salcudean, S.E.: Robotically controlled three-dimensional micro-ultrasound for prostate biopsy guidance. International Journal of Computer Assisted Radiology and Surgery **18**(6), 1093–1099 (2023)
24. You, C., Li, X., Du, Y., Peng, L., Wang, H., Zhang, X., Wang, A.: The microultrasound-guided prostate biopsy in detection of prostate cancer: A systematic review and meta-analysis. Journal of Endourology **36**(3), 394–402 (2022)
25. Zahiri-Azar, R., Salcudean, S.E.: Motion estimation in ultrasound images using time domain cross correlation with prior estimates. IEEE Transactions on Biomedical Engineering **53**(10), 1990–2000 (2006)
26. Zeng, Q., Mohammed, S., Aleef, T.A., Pang, E.H., Hu, C., Jago, J., Rohling, R., Salcudean, S.E.: Multifrequency liver shear wave absolute vibro-elastography with an xmatrix array-2d vs. 3d comparison study. In: 2022 IEEE International Ultrasonics Symposium (IUS). pp. 1–4. IEEE (2022)